© 2017. Published by The Company of Biologists Ltd | Development (2017) 144, 4645-4657 doi:10.1242/dev.158873

RESEARCH ARTICLE

Motor neurons with limb-innervating character in the cervical spinal cord are sculpted by apoptosis based on the Hox code in chick embryo

Katsuki Mukaigasa[1], Chie Sakuma[1], Tomoaki Okada[1], Shunsaku Homma[1], Takako Shimada[1], Keiji Nishiyama[1,*], Noboru Sato[2] and Hiroyuki Yaginuma[1,‡]

ABSTRACT

In the developing chick embryo, a certain population of motor neurons (MNs) in the non-limb-innervating cervical spinal cord undergoes apoptosis between embryonic days 4 and 5. However, the characteristics of these apoptotic MNs remain undefined. Here, by examining the spatiotemporal profiles of apoptosis and MN subtype marker expression in normal or apoptosis-inhibited chick embryos, we found that this apoptotic population is distinguishable by Foxp1 expression. When apoptosis was inhibited, the Foxp1$^+$ MNs survived and showed characteristics of lateral motor column (LMC) neurons, which are of a limb-innervating subtype, suggesting that cervical Foxp1$^+$ MNs are the rostral continuation of the LMC. Knockdown and misexpression of Foxp1 did not affect apoptosis progression, but revealed the role of Foxp1 in conferring LMC identity on the cervical MNs. Furthermore, ectopic expression of Hox genes that are normally expressed in the brachial region prevented apoptosis, and directed Foxp1$^+$ MNs to LMC neurons at the cervical level. These results indicate that apoptosis in the cervical spinal cord plays a role in sculpting Foxp1$^+$ MNs committed to LMC neurons, depending on the Hox expression pattern.

KEY WORDS: Foxp1, Hox, Apoptosis, Neck, Motor neuron, Chick

INTRODUCTION

Motor neurons (MNs) in the spinal cord project their axons to the skeletal muscles and sympathetic ganglia, and are responsible for the central control of body movement and visceral activity in vertebrates. Based on the patterns of axonal trajectories and peripheral targets, spinal MNs can be divided into four major subpopulations that form distinct longitudinal columns within the spinal cord (Dasen and Jessell, 2009; Tsuchida et al., 1994). In brief, MNs that innervate the axial muscles form the medial motor column (MMC), MNs that innervate the body wall muscles form the hypaxial motor column (HMC), MNs that innervate the limb muscles form the lateral motor column (LMC), and visceral MNs that innervate the sympathetic trunk form the preganglionic motor column (PGC, referred to as the column of Terni in chick). The LMC is further divided into two subdivisions: the medial half (LMCm) contains MNs projecting into the ventral limb bud, and the lateral half (LMCl) contains MNs projecting into the dorsal limb bud. Regardless of these subtype diversifications, all spinal MNs are derived from a common progenitor domain, termed pMN, which is defined by the expression of Olig2 in the ventral spinal cord (Mizuguchi et al., 2001; Novitch et al., 2001). Therefore, precise control of the MN subtype specification from the progenitor is of crucial importance for vertebrates to achieve sophisticated behavior. A number of recent studies have provided significant progress in elucidating the molecular mechanisms underpinning spinal MN diversification (Francius and Clotman, 2014; Jessell, 2000; Stifani, 2014). In early stages of neural development, the rostrocaudal identities of neural tube cells are defined by graded fibroblast growth factor (FGF) and retinoid signals derived from Hensen's node and paraxial mesoderm, resulting in the patterned expression of Hox proteins along the rostrocaudal axis (Bel-Vialar et al., 2002; Ensini et al., 1998; Lance-Jones et al., 2001; Liu et al., 2001; Omelchenko and Lance-Jones, 2003). Subsequently, Hox proteins direct segment-specific motor column formations, i.e. the LMCs are formed at limb levels, and the HMC and PGC are formed at the thoracic level (Dasen et al., 2003; Jung et al., 2010, 2014; Misra et al., 2009; Shah et al., 2004; Wu et al., 2008). In contrast, the MMC is generated along the entire spinal cord in a Hox-independent manner; thus, whether to differentiate into MMC neurons or segment-specific MNs should be determined at a certain segment. Such intrasegmental specification of the MN subtype is achieved through a ventral-to-dorsal gradient of Wnt4/5 expression that maintains MMC determinant Lhx3/4 expression (Agalliu et al., 2009), as well as through cross repression between Lhx3/4 and Foxp1, which is a determinant of LMC or PGC fate (Dasen et al., 2008; Rousso et al., 2008).

In the non-limb-innervating cervical spinal cord, phrenic MNs are generated alongside MMC neurons in mammals; however, only MMC neurons are present in chick (Lumsden, 1995; Philippidou et al., 2012; Stifani, 2014). This single columnar organization of the chick cervical spinal cord is suggestive of a simple differentiation of progenitor cells solely into MMC neurons. However, contrary to this prediction, another distinct population of MNs, which display the aspect of cell death, has been recognized in the cervical spinal cord (Levi-Montalcini, 1950; O'Connor and Wyttenbach, 1974; Yaginuma et al., 1996). Occurrence of this cell death is restricted to the cervical region, and between embryonic days (E) 4 and 5 (Levi-Montalcini, 1950; Yaginuma et al., 1996). It was initially postulated that these degenerating MNs within the cervical spinal cord were abortive sympathetic preganglionic neurons (Levi-Montalcini, 1950). Although transplantations of the cervical spinal cord to the thoracic level were performed to test this hypothesis, the identity of

[1]Department of Neuroanatomy and Embryology, School of Medicine, Fukushima Medical University, Fukushima 960-1295, Japan. [2]Division of Gross Anatomy and Morphogenesis, Niigata University Graduate School of Medical and Dental Sciences, Niigata 951-8510, Japan.
*Present address: Faculty of Home Economics, Koriyama Women's University, Fukushima 963-8503, Japan.

‡Author for correspondence (h-yaginm@fmu.ac.jp)

K.M., 0000-0003-3110-5158; H.Y., 0000-0002-5453-4484

Received 18 September 2017; Accepted 16 October 2017

Development (2017) 144, 4645-4657 doi:10.1242/dev.158873

the degenerating MNs was not determined (Shieh, 1951). Several previous studies, including our own, have clarified several characteristics of this neuronal death within the cervical spinal cord. The degenerating MNs show the morphological features of apoptosis, as well as activation of caspase proteins, indicating that these MNs die by apoptosis (O'Connor and Wyttenbach, 1974; Sato et al., 2006; Yaginuma et al., 1996, 2001). Apoptosis of cervical MNs is suppressed by transfection of the anti-apoptotic gene *Bcl-2* (Sato et al., 2002b). Treatments of an array of neurotrophic agents do not alter the apoptosis of MNs in the cervical spinal cord, suggesting that this apoptosis occurs in a cell-autonomous manner (Yaginuma et al., 1996). In spite of these characteristics of apoptosis, whether this degenerating population can be classified as one of the known columnar subtypes or as a novel subtype, and why the apoptosis occurs only in the cervical spinal cord, remain unclear.

In the present study, we demonstrated that apoptotic MNs of the cervical spinal cord can be distinguished by Foxp1 expression. Characterization of MNs expressing Foxp1 after apoptosis inhibition revealed that they exhibit LMC characteristics. Functional analyses of Foxp1 indicated a role for Foxp1 in specifying LMC fate, but not in apoptosis induction in the cervical spinal cord. Moreover, we found that the apoptotic fate of Foxp1$^+$ MNs is affected by Hox misexpression. Our results suggest that Foxp1$^+$ MNs in the cervical spinal cord are homologous to LMC neurons, and are eliminated by apoptosis depending on the Hox expression pattern. We consider these transient Foxp1$^+$ MNs in the cervical spinal cord to be a trail of caudal shift of limb-innervating MNs, which coincides with neck elaboration during vertebrate evolution.

RESULTS

Spatiotemporal profiles of MN marker expression and apoptosis in the developing cervical spinal cord

To determine whether apoptosis of the cervical spinal cord occurs in a specific MN subtype, we first examined the expression of the known MN markers (Isl1/2, Foxp1, Lhx3, Phox2b) simultaneously with activated caspase 3 (Casp3) at Hamburger-Hamilton stage (HH) 24, when the largest number of apoptotic cells is observed. Isl1/2 was used as a marker of all spinal MNs. Foxp1 is a marker for LMC neurons at the brachial and lumbar levels, and for PGC neurons at the thoracic level (Dasen et al., 2008; Rousso et al., 2008). However, its expression has not been reported previously at the cervical level. We found that the expression of Foxp1 overlapped with most of the apoptotic region (Fig. 1A). In contrast, the MMC neuron marker Lhx3 did not overlap with apoptosis (Fig. 1B). Phox2b is a marker for spinal accessory MNs (SACMNs)/dorsal MNs (dMNs), which are derived from the ventral-most progenitor domain, termed p3, in the neural tube, and innervate the cucullaris muscle in chick (Jarrar et al., 2015; Kobayashi et al., 2013). The expression of Phox2b also did not overlap with the apoptotic region (Fig. 1C). We further performed immunohistochemistry in combination with a terminal deoxynucleotidyl transferase-mediated dUTP nick end labeling (TUNEL) assay to determine whether each MN marker colocalizes with the TUNEL signal at the single-cell level. Colocalization of Foxp1 with TUNEL was observed in all examined apoptotic nuclei (Fig. S1, Table S1). By contrast, nuclei exhibiting colocalization of Lhx3 and TUNEL were scarcely detected (Fig. S1, Table S1), indicating that apoptosis does not occur in Lhx3$^+$ MMC neurons.

To confirm the relationship between Foxp1 and apoptosis, temporal patterns of MN marker expression and apoptosis were examined from HH18 to HH27 in the cervical spinal cord. At HH18, most MNs expressed Lhx3, but not Foxp1 (Fig. 1D,J). Several Lhx3$^-$ MNs were considered to be SACMNs/dMNs (Fig. 1J). Foxp1$^+$ MNs were first detectable at HH21, and increased until HH24, whereas Casp3 was first detected in only a few cells at HH23 (Fig. 1E-G,K-M). The number of Foxp1$^+$ and Casp3$^+$ cells peaked at HH24/25, but started to reduce from HH25 onward (Fig. 1G-I,M-O). At HH27, when the topographic organization of the motor columns becomes apparent, the expression of both Foxp1 and Casp3 was extinguished; thus, only MMC neurons (Lhx3$^+$/Isl1/2$^+$) and SACMNs/dMNs (Lhx3$^-$/Isl1/2$^+$) were eventually present at this axial level (Fig. 1I,O). At every stage examined, the expression of Foxp1 was absent from the Lhx3$^+$ MMC neurons, which was consistent with the brachial, thoracic and lumbar levels in chick and mouse spinal cords (Dasen et al., 2008; Morikawa et al., 2009; Rousso et al., 2008). These observations revealed for the first time the presence of the transient population of Foxp1$^+$ MNs, which spatiotemporally overlaps with apoptosis of the cervical spinal cord, implying that Foxp1$^+$ MNs in the cervical spinal cord undergo apoptosis.

Apoptosis inhibition results in the persistence of Foxp1$^+$ MNs

If the Foxp1$^+$ MNs undergo apoptosis, inhibition of apoptosis should lead to the persistence of Foxp1$^+$ MNs even after HH26, when the Foxp1$^+$ MNs almost disappear in normal development (Fig. 1). To test this possibility, we examined the expression of Foxp1 in the *Bcl-2*-electroporated embryos, as apoptosis of the cervical spinal cord is prevented by *Bcl-2* overexpression (Sato et al., 2002b). Bcl-2 expression did not affect the development of Foxp1$^+$ or total MNs before the onset of apoptosis (Fig. 2A-D). At HH26, in contrast to the non-electroporated side or *GFP*-electroporated embryos, in which only a few Foxp1$^+$ MNs were detected, a substantial number of Foxp1$^+$ MNs were observed on the *Bcl-2*-electroporated side (Fig. 2E-H). In our observation of the cervical spinal cord in normal development, much weaker Foxp1 expression was also observed in Phox2b$^+$ SACMNs/dMNs, which did not undergo apoptosis. To clearly distinguish the SACMNs/dMNs from the apoptotic MNs, Phox2b was detected simultaneously with Foxp1 and Isl1/2, and then Foxp1$^+$/Phox2b$^-$ MNs were quantified (Fig. 2I-M). On the *Bcl-2*-electroporated side at HH26, a significantly larger number of Foxp1$^+$/Phox2b$^-$ MNs were observed (18 MNs per 10-µm section on average), compared with the non-electroporated side or *GFP* electroporation (Fig. 2I-M). *Bcl-2* electroporation also increased the total number of MNs to 127% relative to the non-electroporated side (Fig. 2N). These results clearly show that apoptotic MNs in the cervical spinal cord are Foxp1$^+$ MNs.

Foxp1$^+$ MNs that survived after apoptosis inhibition show the characteristics of LMC neurons

We next examined the characteristics of Foxp1$^+$ MNs in the cervical spinal cord after apoptosis inhibition. It is possible that the LMC or PGC identity is assigned to Foxp1$^+$ MNs at the cervical level, as Foxp1 is normally expressed in LMC and PGC neurons. To assess this possibility, the expression of the pan-LMC marker Raldh2 (Aldh1a2), the LMCl marker Lhx1, and the PGC marker phosphorylated-Smad1/5/8 (pSmad) was examined in the Foxp1$^+$ MNs after *Bcl-2* electroporation. The persistent Foxp1$^+$ MNs after apoptosis inhibition displayed Raldh2 and Lhx1 expression, but not pSmad expression, demonstrating that Foxp1$^+$ MNs in the cervical spinal cord exhibit molecular characteristics identical to those of LMC neurons (Fig. 3A-I). Consistent with this, Foxp1$^+$ MNs at the cervical level occupied the lateral portion of the ventral horn after

Development (2017) 144, 4645-4657 doi:10.1242/dev.158873

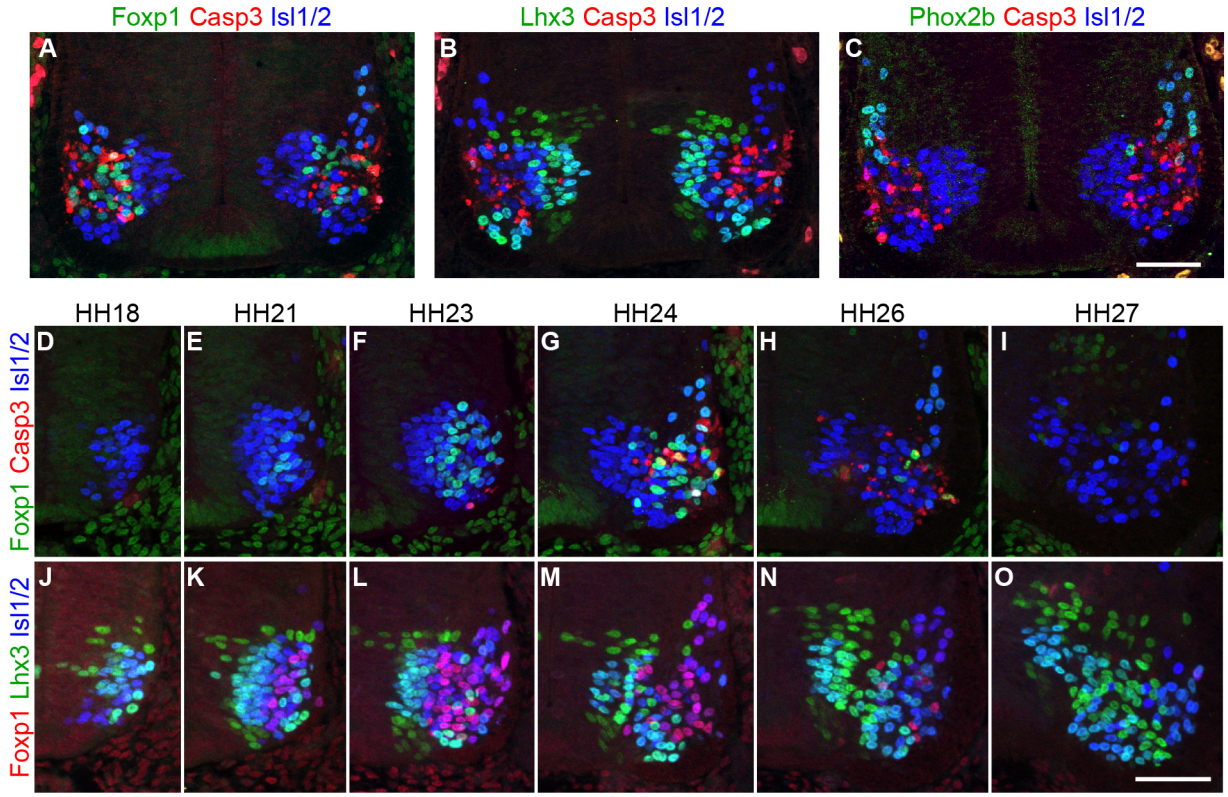

Fig. 1. Spatiotemporal overlap of Foxp1 expression with apoptosis. (A-C) Expression of MN markers and Casp3 was examined by immunohistochemistry in the cervical spinal cord of chick embryos at HH24, indicating that the expression of Foxp1, but not Lhx3 and Phox2b, spatially overlaps with Casp3. (D-O) Immunohistochemistry for Foxp1, Casp3, Isl1/2 (D-I), and for Foxp1, Lhx3, Isl1/2 (J-O) were performed in the cervical spinal cord from HH18 to HH27. The expression of Foxp1 was first detected at HH21 (E,K), increased gradually, and peaked at HH24 (G,M). Correspondingly, the most intense staining of Casp3 was observed at HH24 (G). At HH27, almost all MNs expressed Lhx3, and neither Casp3 nor Foxp1 were detected (I,O). Scale bars: 50 µm (in C for A-C; in O for D-O).

apoptosis inhibition similarly to LMC neurons (Fig. 2K,L, Fig. 3A, D,G), clearly contrasting with PGC neurons, which migrate dorsomedially in chick (Fig. S2; Levi-Montalcini, 1950). For further elucidation of the characteristics of Foxp1$^+$ MNs in the cervical spinal cord, we next examined the axonal trajectory in the cervical region by immunohistochemistry for Raldh2, as this protein is expressed in Foxp1$^+$ MNs and is detectable in the somata, dendrites and axons (Berggren et al., 1999). Raldh2$^+$ axons on the *Bcl-2*-electroporated side projected ventrolaterally beyond the myotome, which is marked by myosin heavy chain (MyHC) expression; however, Raldh2$^+$ axons were not observed in the dorsal ramus (Fig. 3J-P). To confirm this axonal trajectory, retrograde tracing using biotinylated-dextran amine (BDA) was performed at HH26/27 in the *Bcl-2*-electroporated embryo, after the dorsal roots were cut in order to trace axons in the ventral root only. When BDA was injected into the ventrolateral region of the neck, the Foxp1$^+$ MNs that survived in the cervical spinal cord were retrogradely labeled (Fig. 3Q). A few Lhx3$^+$ MNs were also labeled. They are supposed to be MNs innervating the longus colli muscles (Luxenhofer et al., 2014), and probably have not yet branched from the ventral ramus at this stage. On the other hand, when the dorsal ramus was traced retrogradely, only Lhx3$^+$ MNs, but not Foxp1$^+$ MNs, were labeled by BDA (Fig. 3R). These results demonstrate that Foxp1$^+$ MNs in the cervical region project their axons along the ventral ramus to the ventrolateral region of the neck. We also carried out whole-mount immunostaining for neurofilament (NF) to examine the axonal trajectories in whole embryos. However, aberrant axonal projections were not observed in the *Bcl-2*-electroporated embryos, suggesting that the axons of Foxp1$^+$ MNs follow the normal pattern of the cervical spinal nerve (Fig. 3S,T). Although the extent to which this axonal trajectory is related to that of LMC neurons is unclear, these results reject the hypothesis that Foxp1$^+$ MNs that die by apoptosis at the cervical level are classified as MMC or PGC neurons. Taken together, Foxp1$^+$ MNs at the cervical level are most closely related to LMC neurons.

Foxp1 knockdown does not affect apoptosis in the cervical spinal cord

Our results demonstrate that Foxp1$^+$ MNs in the cervical region not only undergo apoptosis, but also exhibit LMC characteristics such as cell body position and marker expression, raising the question of whether Foxp1 functions as an inducer of apoptosis, a determinant of LMC fate, or both. To explore the function of Foxp1 at the cervical level, we first carried out Lhx3 misexpression, which has been reported to suppress Foxp1 expression (Dasen et al., 2008; Rousso et al., 2008). After Lhx3 misexpression, the apoptotic cells were decreased at HH25; however, the Foxp1$^+$ MNs themselves were also decreased before the onset of apoptosis (Fig. S3). This made it difficult to determine whether the decrease of apoptosis is attributed to insufficient expression of Foxp1, suggesting that Lhx3 misexpression is inadequate for direct functional analysis of Foxp1. Next, for the specific downregulation of Foxp1, we prepared a *Foxp1* shRNA (Foxp1-sh) expression vector (Materials and Methods). At first, the extent of *Foxp1* knockdown by the induction of Foxp1-sh was evaluated at HH23, when apoptosis

Development (2017) 144, 4645-4657 doi:10.1242/dev.158873

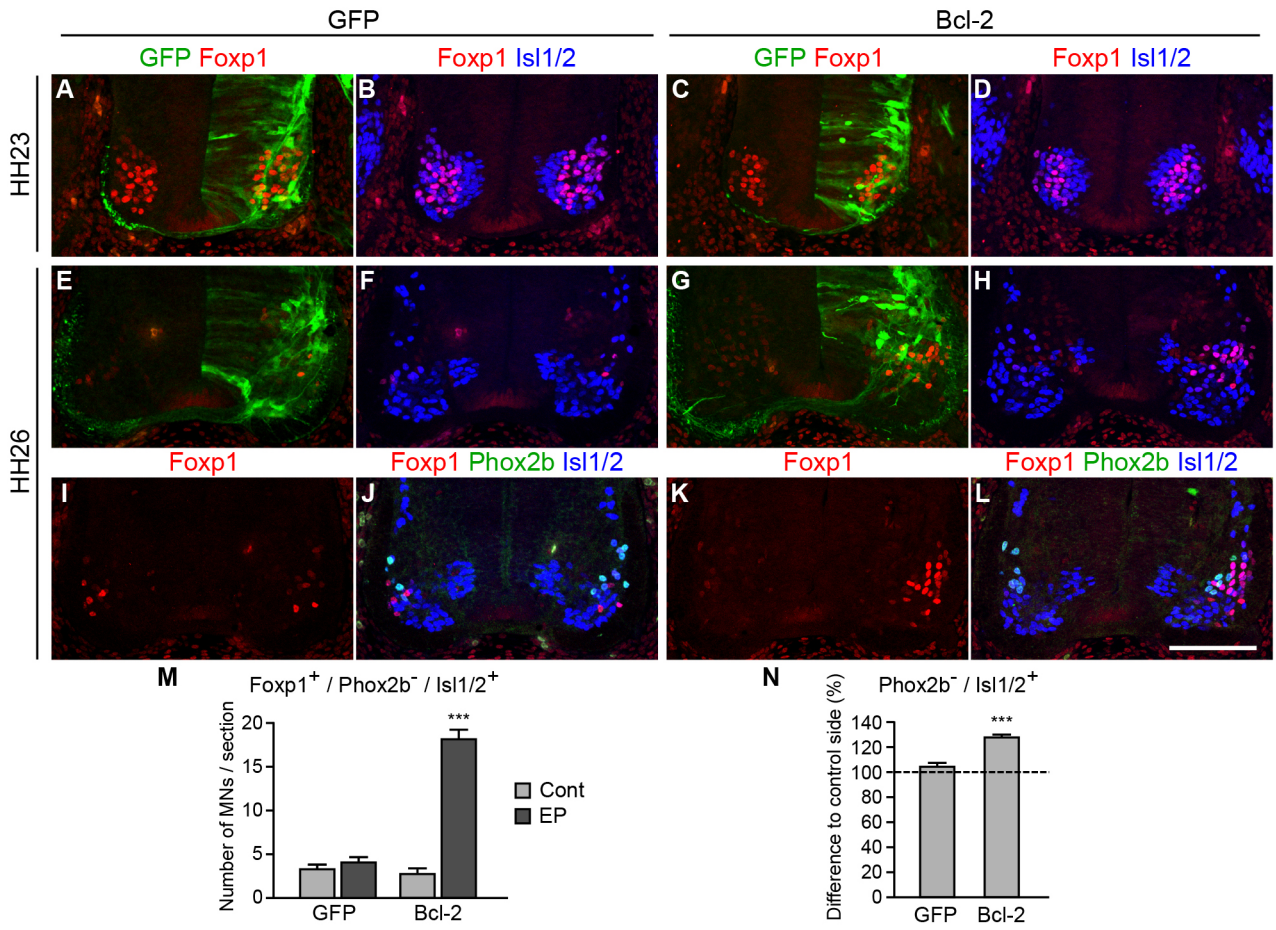

Fig. 2. Apoptosis inhibition by Bcl-2 leads to the persistence of Foxp1$^+$ MNs. (A-H) Immunohistochemistry for GFP, Foxp1 and Isl1/2 was performed at HH23 (A-D) or HH26 (E-H) after *GFP* or *Bcl-2* electroporation. *Bcl-2* overexpression did not affect the development of MNs at HH23. At HH26, a substantial number of Foxp1$^+$ MNs were present on the *Bcl-2*-electroporated side, but not in the *GFP*-electroporated embryo. (I-L) The expression of Phox2b, which is a marker for SACMNs/dMNs, was examined simultaneously with Foxp1 and Isl1/2 at HH26 after *GFP* or *Bcl-2* electroporation. (M) Quantification of Foxp1$^+$/Phox2b$^-$/Isl1/2$^+$ MNs at HH26 after electroporation. Average numbers of MNs per 10-µm section on the non-electroporated (Cont) or electroporated (EP) side are shown. (N) Quantification of Phox2b$^-$/Isl1/2$^+$ MNs at HH26 after *GFP* or *Bcl-2* electroporation. Relative differences of the electroporated side to the non-electroporated side are presented. Sample sizes (*n*) are presented as the number of sections examined/the number of embryos examined. *n*=17/5 (GFP), 16/4 (Bcl-2). Values are mean±s.e.m. ***P<0.001 (two-tailed *t*-test). Scale bar: 100 µm.

had not yet commenced (Fig. S4). Whereas the organization of the MNs was unaffected by the induction of control shRNA (Cont-sh), Foxp1$^+$ MNs were significantly decreased and, consequently, Foxp1$^-$/Lhx3$^-$ MNs were increased by Foxp1-sh induction (Fig. S4A-G). The total number of Isl1/2$^+$ MNs was also slightly decreased, whereas Lhx3$^+$ MMC neurons were unaffected by Foxp1-sh induction (Fig. S4G). The knockdown effect of Foxp1-sh was also confirmed in the cultured cell line (Fig. S4H). These results confirmed that *Foxp1* expression is specifically knocked down by Foxp1-sh induction.

Using this shRNA, *Foxp1* knockdown was carried out. To examine whether apoptosis progression was influenced by *Foxp1* knockdown, the number of Lhx3$^-$/Phox2b$^-$ MNs was quantified from HH23 to HH27, as Foxp1$^+$ apoptotic MNs are exclusive of Lhx3$^+$ MMC neurons and Phox2b$^+$ SACMNs/dMNs, and thus correspond to Lhx3$^-$/Phox2b$^-$ MNs (Fig. 4A,B,D,E,G). At HH23, after *Foxp1* knockdown, the number of Lhx3$^-$/Phox2b$^-$ MNs on the electroporated side was lower than that on the non-electroporated side (Fig. 4G). This means that, before the beginning of apoptosis, prospective apoptotic MNs were reduced by *Foxp1* knockdown. The decrease in the number of Lhx3$^-$/Phox2b$^-$ MNs after *Foxp1* knockdown is consistent with the phenotype of *Foxp1* knockout mice, in which a decrease in the number of MNs is detected in the brachial spinal cord at E13.5 (Dasen et al., 2008). At later stages, the number of Lhx3$^-$/Phox2b$^-$ MNs gradually decreased as development proceeded, and almost disappeared at HH27 both in Foxp1-sh and Cont-sh induction groups (Fig. 4G). These results demonstrate that apoptosis is executed even after *Foxp1* knockdown, and are inconsistent with the idea that Foxp1 functions as an inducer of apoptosis. We also performed the TUNEL assay at HH25 after *Foxp1* knockdown. The number of TUNEL-positive nuclei was decreased by approximately 30% compared with the non-electroporated side (Fig. 4C,F,H); however, this amount of reduction in apoptosis can be attributed to the decrease in the number of Lhx3$^-$/Phox2b$^-$ MNs at HH23 after *Foxp1* knockdown (Fig. 4G). This implies a substantial progress of apoptosis.

Foxp1 does not induce apoptosis, but rather confers LMC identity in the cervical spinal cord

For further evaluation of the role of Foxp1 in the cervical spinal cord, we next induced misexpression of Foxp1 utilizing a 5′ upstream sequence of the mouse *Hb9* gene (*Mnx1*), which is exclusively expressed in postmitotic MNs (Arber et al., 1999; Thaler et al., 1999). The plasmid vector containing the *Hb9* upstream sequence and

Development (2017) 144, 4645-4657 doi:10.1242/dev.158873

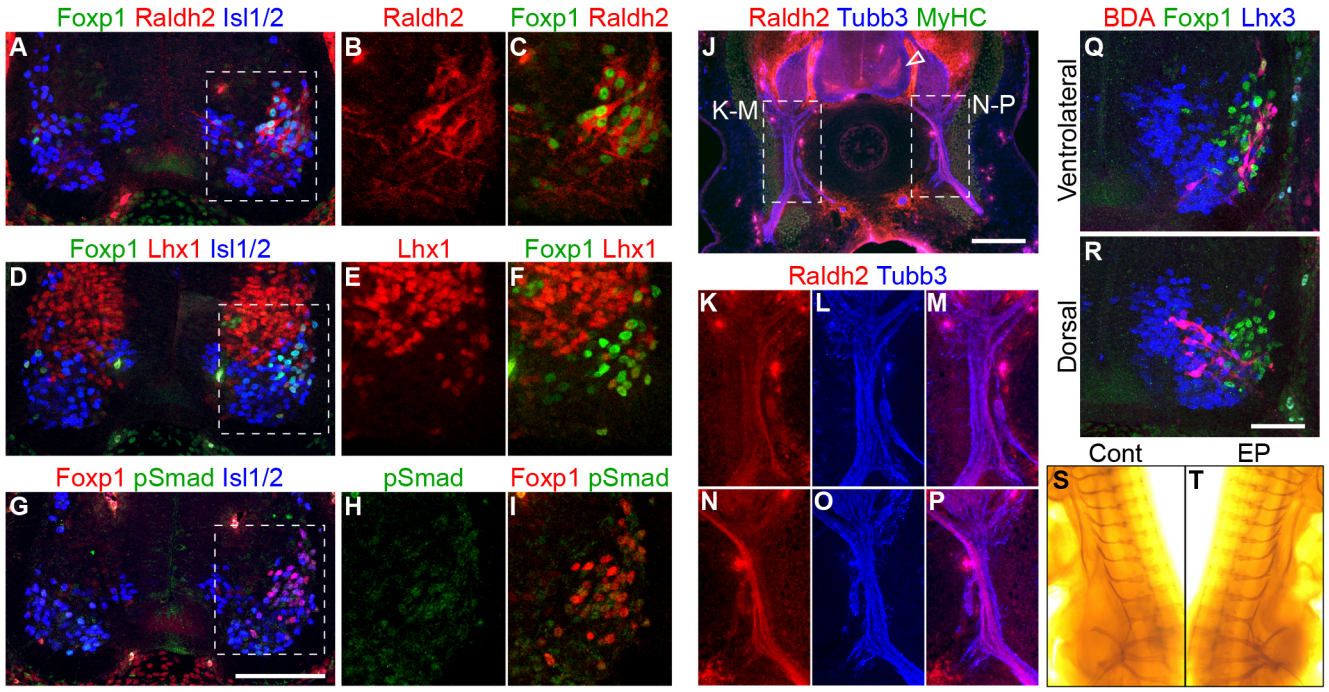

Fig. 3. Foxp1$^+$ MNs of the cervical spinal cord show the characteristics of LMC neurons. (A-I) Expression of MN subtype markers at HH27 in the cervical spinal cord of the *Bcl-2*-electroporated embryo. Boxed area in A, D and G are enlarged in B,C, E,F and H,I, respectively. The LMC marker Raldh2 and the LMCl marker Lhx1 were detected in Foxp1$^+$ MNs in the *Bcl-2*-electroporated embryo. The expression of pSmad, which is a marker of PGC neurons, was not observed in the Foxp1$^+$ MNs at the cervical level after *Bcl-2* electroporation. (J) Immunohistochemistry for Raldh2, tubulin beta 3 class III (Tubb3) and MyHC at mid-cervical level in the *Bcl-2*-electroporated embryo. The electroporated half of the spinal cord is on the right side in this image. The expression of Raldh2 was increased in the *Bcl-2*-electroporated side of the spinal cord (arrowhead). Raldh2$^+$ axons projected along the ventral root, and extended beyond the myotome. Boxed areas around the ventral ramus of the non-electroporated and electroporated side are enlarged in K-M and N-P, respectively. (Q,R) Retrograde tracing by BDA in the *Bcl-2*-electroporated embryo at HH26/27. BDA was injected into the ventrolateral neck region (Q) or the dorsal ramus (R). Immunohistochemistry for Foxp1 and Lhx3 was then performed. Foxp1$^+$ MNs were retrogradely labeled after BDA injection into the ventrolateral neck region (Foxp1$^+$ MNs/BDA$^+$ MNs=63/140 in a total of 14 sections from 5 embryos). Only Lhx3$^+$ MNs were labeled by retrograde tracing of the dorsal ramus (Foxp1$^+$ MNs/BDA$^+$ MNs=0/181 in a total of 16 sections from 5 embryos). (S,T) Whole-mount chick embryo was labeled with anti-NF antibody at HH27 after *Bcl-2* electroporation. Dorsolateral view from non-electroporated (Cont) or electroporated (EP) side of the same embryo from the cervical to brachial levels. Rostral to the top. Scale bars: 100 µm (in G for A,D,G); 200 µm (J); 50 µm (in R for Q,R).

Myc-tagged *Foxp1* coding sequence (*Hb9:Foxp1-Myc*) was electroporated in the cervical spinal cord, and MN marker expression and apoptosis were then examined from HH20 to HH27. At HH20, when the expression of Foxp1 had not yet started in normal development (Fig. 1), induced expression of Foxp1 was detected on the electoroporated side (Fig. 5A). Despite this earlier expression of Foxp1, the temporal profile of Casp3 remained unaltered (Fig. 5A-F). Furthermore, at HH27, when Foxp1$^+$ MNs have disappeared in normal development, a large number of Foxp1$^+$ MNs were present on the electroporated side, but did not exhibit Casp3 activation (Fig. 5G, H). We also performed the TUNEL assay and demonstrated that the number of TUNEL-positive nuclei at HH24/25 was unaltered by Foxp1 misexpression (Fig. 5O-Q). These results indicate that Foxp1 neither induces apoptosis nor determines its timing.

To clarify the consequences of Foxp1 misexpression at the cervical level in more detail, we examined Foxp1 expression within and outside the Lhx3$^+$ MMC neurons after *Hb9:Foxp1-Myc* electroporation. Foxp1 is not expressed in Lhx3$^+$ MMC neurons in normal development (Fig. 1). In contrast, Foxp1 was ectopically induced in Lhx3$^+$ MMC neurons after the electroporation, thus generating Foxp1$^+$/Lhx3$^+$ MNs (Fig. 5I,J,R). At HH26/27, the number of Foxp1$^+$/Lhx3$^-$ MNs, the molecular identity of which is normal apoptotic MNs, was reduced compared with HH24 both on the non-electroporated and electroporated sides (Fig. 5I-L,R). On the other hand, Foxp1$^+$/Lhx3$^+$ MNs (Foxp1 ectopically induced MNs) were persistent on the electroporated side at a comparable level to HH24 (Fig. 5K,L,R). These results again indicate that Foxp1 does not induce apoptosis. A minor increase in Foxp1$^+$/Lhx3$^-$ MNs on the electroporated side at HH26/27 can probably be attributed to a loss of Lhx3 expression in MMC neurons following Foxp1 misexpression because of the cross-repressive relationship between Foxp1 and Lhx3 (Dasen et al., 2008; Morikawa et al., 2009; Rousso et al., 2008). In fact, the number of Lhx3$^+$ MNs was reduced by Foxp1 misexpression (Fig. 5S).

These results show that Foxp1 is not a trigger of apoptosis, and consequently raise the possibility that Foxp1 plays a role in conferring LMC identity on cervical MNs. To verify this possibility, the expression of LMC markers was examined after Foxp1 misexpression. At HH27, LMC markers Raldh2 and Lhx1 were expressed in the MNs in which Foxp1 was ectopically induced, indicating that Foxp1 functions as a determinant of LMC fate also at the cervical level (Fig. 5M,N).

Hoxc6 misexpression alters the fate of Foxp1$^+$ MNs in the cervical spinal cord

Despite the functional analysis of Foxp1 in the cervical spinal cord, the molecular mechanism of apoptosis regulation is still unclear. Considering that apoptosis occurs only in the cervical region despite broad Foxp1 expression along the spinal cord (Fig. 6A,B), the mechanism by which apoptosis is limited to the cervical region is

Development (2017) 144, 4645-4657 doi:10.1242/dev.158873

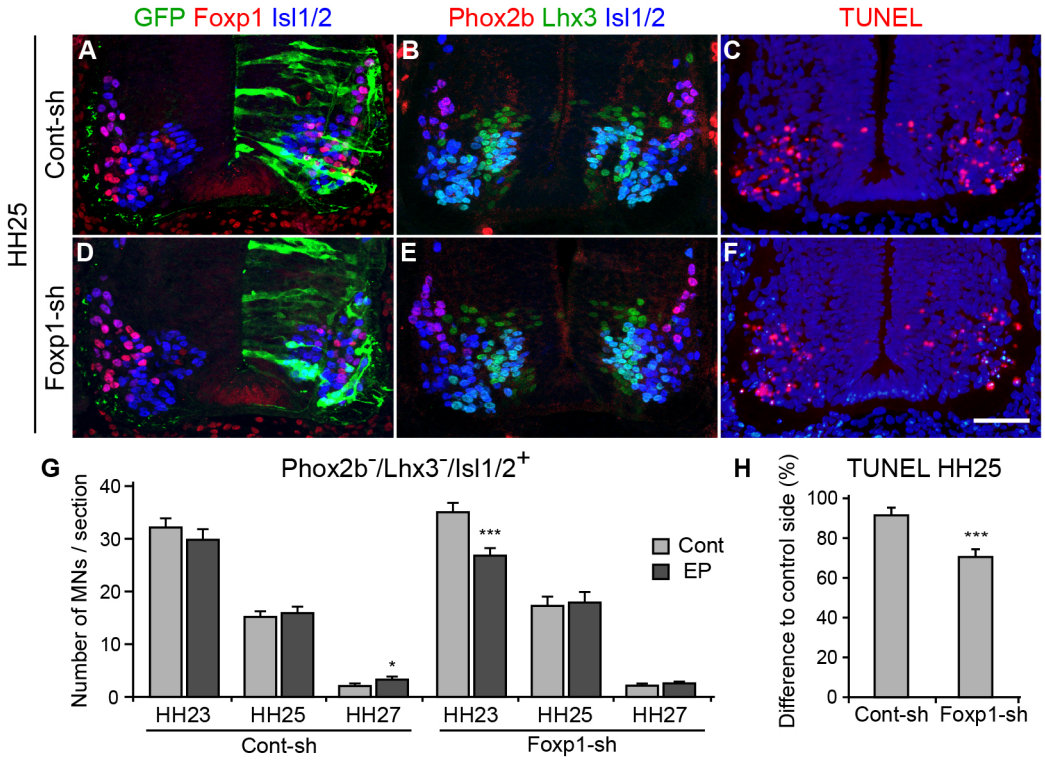

Fig. 4. Apoptosis in the cervical spinal cord is normally executed even after shRNA-mediated *Foxp1* knockdown. (A-F) Immunohistochemistry for GFP, Foxp1, Isl1/2 (A,D), and Phox2b, Lhx3, Isl1/2 (B,E) and TUNEL assay (C,F) at HH25 after Cont-sh or Foxp1-sh induction. (G) Quantification of Phox2b^{-}/Lhx3^{-}/Isl1/2^{+} (equivalent to Foxp1^{+}) MNs at HH23, HH25 and HH27 after electroporation. The number of Phox2b^{-}/Lhx3^{-} MNs decreased gradually both in the Cont-sh- and Foxp1-sh-induced embryos. Average numbers of MNs per 10-µm section on the non-electroporated (Cont) or electroporated (EP) side are shown. *n*=21/6 (Cont-sh at HH23), 18/5 (Cont-sh at HH25), 18/5 (Cont-sh at HH27), 25/7 (Foxp1-sh at HH23), 27/8 (Foxp1-sh at HH25), 16/5 (Foxp1-sh at HH27). (H) Quantification of TUNEL-positive nuclei at HH25 after electroporation. Percentage changes in the number of TUNEL-positive nuclei on the electroporated side compared with that on the non-electroporated side are presented. *n*=35/9 (Cont-sh), 30/10 (Foxp1-sh). Values are mean±s.e.m. **P*<0.05; ****P*<0.001 (two-tailed *t*-test). Scale bar: 50 µm (in F for A-F).

predicted to be independent of Foxp1 activity. Hox proteins are expressed in discrete rostrocaudal positions within the spinal cord, and endow spinal MNs with positional identity (Dasen et al., 2003; Jung et al., 2010, 2014; Misra et al., 2009; Shah et al., 2004; Wu et al., 2008), so Hox proteins are the most likely candidates responsible for the regional regulation of apoptosis. Thus, we next explored the relevance of Hox proteins to apoptosis regulation. Hoxc6 expression is congruent with the brachial LMC region (Dasen et al., 2003), and we found that the cervical apoptotic region was bordered caudally by Hoxc6 expression (Fig. 6C,D, Fig. S5), raising the possibility that Hoxc6 plays a role in the suppression of apoptosis. To test this hypothesis, we ectopically induced *Hoxc6* to the cervical spinal cord by electroporation. At HH24, after ectopic expression of *Hoxc6*, the topographic distribution of Foxp1^{+} MNs was almost normal. However, the Foxp1 expression level was slightly increased, and apoptosis was reduced in the electroporated side (Fig. 6E-H,M). At HH27, in contrast to the non-electroporated side, in which Foxp1^{+} MNs had already disappeared, Foxp1^{+} MNs were present and expressed LMC marker Raldh2 in the *Hoxc6*-electroporated side (Fig. 6I-L,N). These results demonstrate that Hoxc6 prevented Foxp1^{+} MNs from undergoing apoptosis and directed them to LMC fate.

Hox paralog group 6-8 proteins act redundantly to prevent apoptosis

To confirm that Hoxc6 prevents apoptosis of the Foxp1^{+} MNs, *Hoxc6* knockdown was performed using shRNA. A *Hoxc6* shRNA expression vector was constructed (Materials and Methods) and was electroporated in the boundary region of the cervical and brachial spinal cord; the apoptotic region was then examined at HH25. If Hoxc6 alone functions as a repressor of apoptosis, the apoptotic region should be extended caudally by *Hoxc6* knockdown. However, the apoptotic region remained unaltered compared with the non-electroporated side (Fig. S6). Considering that paralogous Hox genes have redundant functions in several cases (Wellik, 2007), this result suggests that other Hox proteins expressed in the brachial region can compensate for the lack of Hoxc6. To examine the function of the other Hox proteins regarding the prevention of apoptosis, seven Hox genes expressed around the brachial region (*Hoxa4*, *Hoxc4*, *Hoxa5*, *Hoxc5*, *Hoxa6*, *Hoxa7*, *Hoxc8*) were induced in the cervical region by electroporation, and the fate of the Foxp1^{+} MNs was examined. Although a few Foxp1^{+} MNs were observed after forced expression of *Hoxc4*, Foxp1^{+} MNs in the cervical spinal cord mostly disappeared at HH27, as in normal development, after forced expression of Hox paralog group 4 and 5 genes (Fig. 7A-H). In contrast, forced expression of *Hoxa6*, *Hoxa7* and *Hoxc8* resulted in the persistence of Foxp1^{+} MNs similarly to the case of Hoxc6 (Fig. 7I-N). These results show that the Hox proteins in paralog group 6-8 act redundantly to prevent apoptosis of the Foxp1^{+} MNs.

Ectopic expression of Hoxc6 in the cervical spinal cord does not interfere with the expression of Hox paralog group 5 genes

Hoxc9, which is expressed in the thoracic spinal cord, can block brachial LMC specification through the repression of Hox genes

Development (2017) 144, 4645-4657 doi:10.1242/dev.158873

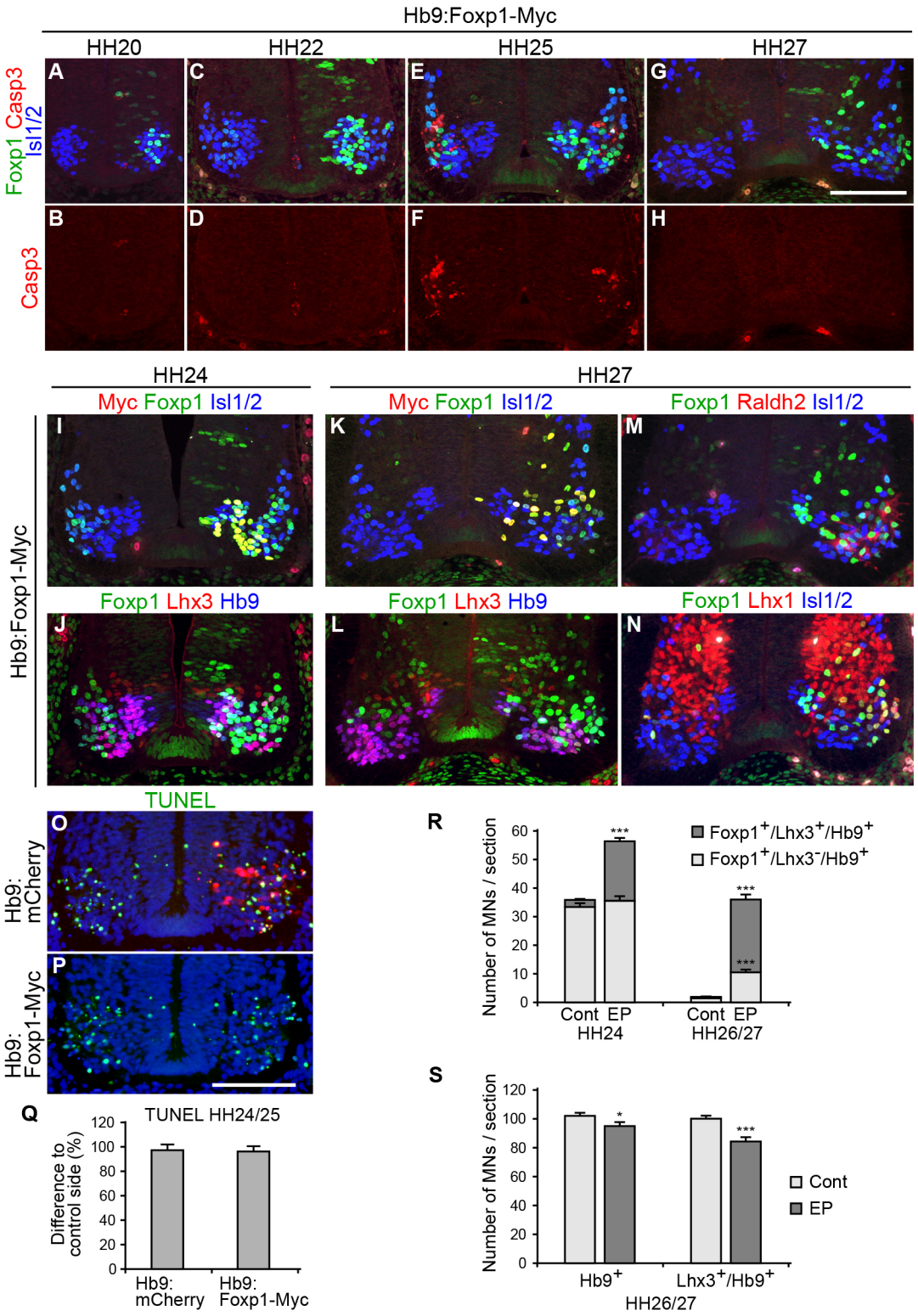

Fig. 5. See next page for legend.

expressed in the brachial region, indicating that the caudal border of the brachial LMC is shaped by Hox cross-repressive interaction (Dasen et al., 2003; Jung et al., 2010). It is possible that a similar mechanism participates in the regulation of the cervical apoptotic region. Thus, we speculated that the prevention of apoptosis by the ectopic expression of Hoxc6 is mediated through the repression of Hox genes expressed in the cervical Foxp1^{+} MNs. To examine this hypothesis, the endogenous expression of Hox proteins in the Foxp1^{+} MNs at cervical level was examined after *Hoxc6* electroporation. We confirmed that Hoxa5 and Hoxc5 were expressed in almost all Foxp1^{+} MNs at the cervical level at HH24 in normal development (Fig. 8B,C). Contrary to expectations,

Development (2017) 144, 4645-4657 doi:10.1242/dev.158873

Fig. 5. Misexpression of Foxp1 does not induce apoptosis, but rather confers the LMC identity on MNs of the cervical spinal cord.
(A-H) Immunohistochemistry for Casp3, Foxp1 and Isl1/2 was performed at HH20 (A,B), HH22 (C,D), HH25 (E,F) and HH27 (G,H) after electroporation of *Hb9:Foxp1-Myc*. Foxp1 was detected throughout these stages on the electroporated side, differing from the transient presence of Foxp1$^+$ MNs on the non-electroporated side. Nevertheless, Casp3 was observed only around HH25 both on the electroporated and non-electroporated sides.
(I-L) Immunohistochemistry for Myc, Foxp1, Isl1/2 (I,K), and Foxp1, Lhx3, Hb9 (J,L) were performed at HH24 and HH27. At HH24, ectopically induced Foxp1, which was highly expressed especially in the Lhx3$^+$ MMC region, was detected by anti-Myc or anti-Foxp1 antibodies. At HH27, although Foxp1$^+$ MNs had already disappeared on the non-electroporated side, a large number of Myc$^+$/Foxp1$^+$ MNs were observed on the *Hb9:Foxp1-Myc* electroporated side. (M,N) The LMC markers Raldh2 and Lhx1 were detected in MNs in which Foxp1 was ectopically induced. (O,P) TUNEL assay at HH24 after *Hb9:mCherry* or *Hb9:Foxp1-Myc* electroporation. (Q) Quantification of TUNEL-positive nuclei at HH24/25 after electroporation. Percentage changes in the number of TUNEL-positive nuclei on the electroporated side compared with that on the non-electroporated side are shown. The number of TUNEL-positive nuclei was unaltered by *Hb9:mCherry* and *Hb9:Foxp1-Myc* electroporation. *n*=19/5 (Hb9:mCherry), 24/7 (Hb9:Foxp1-Myc). (R,S) Quantification of MNs in the cervical spinal cord after *Hb9:Foxp1-Myc* electroporation. Average numbers of MNs exhibiting the indicated expression pattern of markers per 10-µm section on the non-electroporated (Cont) or electroporated (EP) side are shown. *n*=21/6 (HH24), 25/7 (HH26/27). Values are mean±s.e.m. **P*<0.05, ****P*<0.001 (two-tailed *t*-test). Scale bars: 100 µm (in G for A-H; in P for I-P).

however, the expression of Hoxa5 and Hoxc5 in the Foxp1$^+$ MNs was maintained at HH24 after *Hoxc6* electroporation (Fig. 8A-C,G,H). Furthermore, Hoxa5 and Hoxc5 were also expressed in the persistent Foxp1$^+$ MNs at HH27 after the electroporation (Fig. 8D-F). These results suggest that ectopic expression of Hoxc6 in the cervical spinal cord prevents apoptosis of the Foxp1$^+$ MNs, but does not interfere with the expression of other Hox genes.

DISCUSSION

Identity of MNs that undergo apoptosis in the cervical spinal cord of chick embryos

Cell death confined to the cervical spinal cord of developing chick embryos was first described by Levi-Montalcini in 1950 (Levi-Montalcini, 1950). Based on the finding that rami communicantes branching from the ventral roots of cervical spinal nerves toward the sympathetic primordia were transiently observed between E3 and E4, the author contended that degenerating MNs were homologous to the sympathetic preganglionic neurons of the thoracic spinal cord. To verify this contention, Shieh performed transplantation of the neural tube from the cervical level to the thoracic level, but did not determine the classification of the degenerating MNs (Shieh, 1951). Since then, the identity of degenerating MNs in the cervical spinal cord has barely been studied for more than 50 years. On the other hand, we previously examined the axonal trajectory of degenerating MNs by retrograde tracing, speculating that these degenerating MNs belong to somatic but not visceral MN populations (Yaginuma et al., 1996). In the present study, we corroborated this speculation and concluded that degenerating MNs in the cervical spinal cord are distinguishable by Foxp1 expression, and are homologous to LMC neurons. This conclusion is based on the following results: (1) during normal development of chick embryos, Foxp1$^+$ MNs existed transiently between HH21 and HH25, and the distribution of the Foxp1$^+$ MNs overlapped with that of apoptosis in the cervical spinal cord (Fig. 1); (2) when apoptosis was inhibited by Bcl-2, Foxp1$^+$ MNs persisted beyond the developmental stage at which Foxp1$^+$ MNs normally disappear (Fig. 2); (3) the LMC markers Raldh2 and Lhx1 were expressed in Foxp1$^+$ MNs that survived after apoptosis inhibition (Fig. 3); (4) axons of Foxp1$^+$/Raldh2$^+$ MNs passed through ventral roots and extended along the ventral ramus after apoptosis inhibition (Fig. 3).

In contrast, apoptosis was not observed in Lhx3$^+$ MNs (Fig. 1, Fig. S1, Table S1). Furthermore, Foxp1$^+$ MNs that survived after apoptosis inhibition occupied lateral, but not dorsomedial, positions in the spinal cord, and neither expressed pSmad nor projected their axons to the dorsal ramus or sympathetic trunk (Fig. 3, Fig. S2). These results indicate that MNs that undergo apoptosis are distinct from MMC or PGC neurons. As HMC neurons at the thoracic level do not express Foxp1 (Dasen et al., 2008; Rousso et al., 2008), it is improbable that the Foxp1$^+$ apoptotic MNs in the cervical spinal cord are the same subtype as HMC neurons. Furthermore, mammalian-specific phrenic MNs also do not express Foxp1 (Philippidou et al., 2012), denying the homology between apoptotic MNs in the cervical spinal cord of chick and phrenic MNs in mammals.

Collectively, Foxp1$^+$ apoptotic MNs of the cervical spinal cord can be considered as the rostral continuation of the LMC. Thus, morphogenesis of the spinal MNs in the cervical region is supposed to proceed in two steps: LMCs are first generated from the rostral cervical level to the caudal brachial level, and then LMCs within the non-limb-innervating region are sculpted by apoptosis (Fig. S7).

The regulation of apoptosis and boundary formation in the spinal cord mediated by Hox transcription factors

In the current study, it was demonstrated that misexpression of Hox paralog group 6-8 genes resulted in the generation of Foxp1$^+$ LMC neurons in the cervical spinal cord. As MMC specification is Hox-independent (Agalliu et al., 2009; Jung et al., 2014; Rousso et al., 2008), MMC neurons are unlikely to be converted to Foxp1$^+$ MNs after Hox6-8 misexpression. Rather, the fate of Foxp1$^+$ apoptotic MNs in the cervical spinal cord is likely to be converted to LMC neurons by Hox6-8 misexpression. This result provides the first evidence that Hox transcription factors contribute to the regional control of cervical apoptosis along the rostrocaudal axis. On the other hand, the apoptotic fate of the Foxp1$^+$ MNs was unaffected by forced expression of Hox4-5 in the cervical spinal cord (Fig. 7). This result suggests that Hox4-5 are permissive to apoptotic signals. Alternatively, it is possible that some of Hox paralog group 4-5 proteins induce pro-apoptotic genes, and apoptosis is executed only in MNs that do not express Hox6-8.

During normal chick embryo development, expression of Hox6 in the spinal MNs is confined to the brachial region, and Hox4-5 are expressed from the cervical to the mid-brachial level (Dasen et al., 2005; Philippidou and Dasen, 2013). Therefore, the expression of Hox paralog group 4-6 genes overlaps with each other at the brachial level, suggesting little or no cross-repressive interaction. The result of rostral misexpression of Hoxc6 in the present study supports this idea also at the cervical level, and suggests that Hoxc6 is capable of disrupting the apoptotic pathway in the cervical region, leaving the expression of other Hox genes unaltered (Fig. 8). In contrast, Hoxc9 represses multiple Hox genes expressed in the brachial region, partitioning the brachial and thoracic region in the spinal cord (Dasen et al., 2003; Jung et al., 2010). These findings and the results of our study show that the rostral and caudal borders of the brachial LMC are established by distinct mechanisms.

Why Foxp1$^+$ MNs are transiently formed in the neck

The present study demonstrated the developmental process of MNs in the chick cervical spinal cord, but it is of particular interest why Foxp1$^+$ MNs are transiently generated in the cervical spinal cord

Development (2017) 144, 4645-4657 doi:10.1242/dev.158873

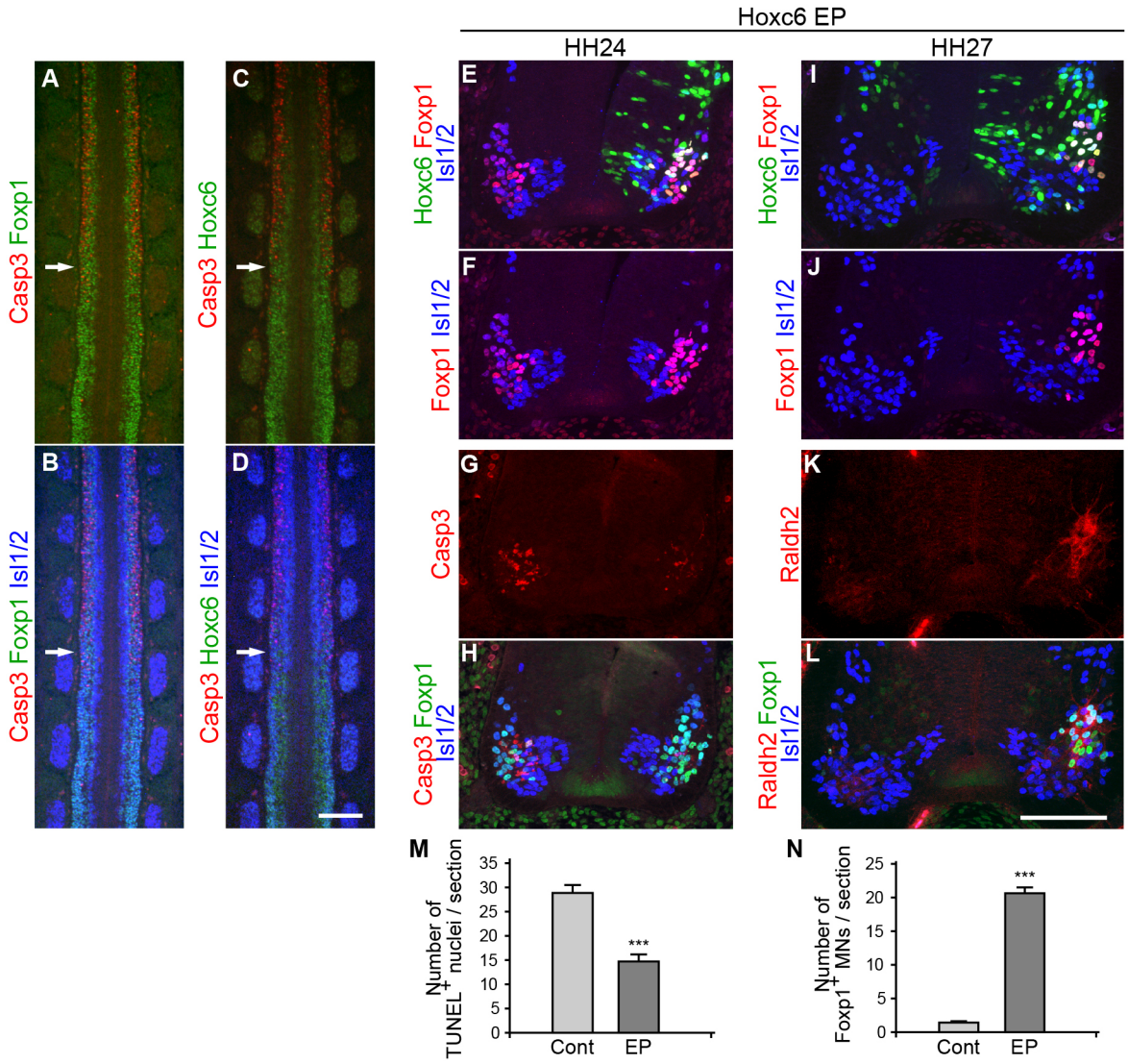

Fig. 6. Ectopic expression of Hoxc6 results in prevention of apoptosis and specification of LMC neurons in the cervical spinal cord. (A-D) Immunohistochemistry for Casp3, Foxp1, Isl1/2 (A,B) and Casp3, Hoxc6, Isl1/2 (C,D) in horizontal longitudinal sections at HH24. Arrows indicate the approximate boundary between the cervical and brachial region of the spinal cord. Rostral to the top. Unlike Foxp1, Hoxc6 was not expressed in Casp3$^+$ cervical MNs. (E-L) Expression of MN markers was examined at HH24 (E-H) and HH27 (I-L) after ectopic expression of Hoxc6. At HH24, topographic distribution of Foxp1$^+$ MNs was not altered, but apoptosis was reduced by Hoxc6 misexpression. At HH27, Foxp1$^+$ MNs were observed in the *Hoxc6*-electroporated side, but not in the non-electroporated side. Foxp1$^+$ MNs in the *Hoxc6*-electroporated side expressed the LMC marker Raldh2. (M,N) Quantification of TUNEL-positive nuclei at HH25 (M) or Foxp1$^+$ MNs at HH27 (N) after electroporation. Average numbers of TUNEL-positive nuclei or Foxp1$^+$ MNs per 10-µm sections on the non-electroporated (Cont) or electroporated (EP) sides are shown. n=14/4 (M), 19/6 (N). Values are mean±s.e.m. ***P<0.001 (two-tailed t-test). Scale bars: 200 µm (in D for A-D); 100 µm (in L for E-L).

despite their eventual disappearance. As we discuss below, it is supposed that the transient Foxp1$^+$ LMC-like neurons in the cervical spinal cord is a trail of caudal shift of limb-innervating MNs in the process of neck elaboration in vertebrate evolution. Early jawless vertebrates, the Osteostraci, had pectoral fins that articulated directly to a head shield, indicating that they had no neck (Janvier, 1996). A fully functional neck appeared in late Devonian tetrapodomorph fish, such as *Tiktaalik roseae*, because they had no bony connection between the skull and the pectoral girdle (Daeschler et al., 2006; Shubin et al., 2006). An elongated movable neck had evolved in amniotes by shifting the shoulder girdle and forelimb caudally (Burke et al., 1995; Ericsson et al., 2013; Nagashima et al., 2016). Based on a comparative anatomical investigation, it has been reported that, in fish, MNs innervating pectoral fins originate in the region straddling hindbrain and spinal cord, unlike the spinal-only origin of forelimb-innervating MNs in tetrapods (Ma et al., 2010). This implies that forelimb-innervating MNs also shifted caudally during vertebrate evolution (Ma et al., 2010). Our findings support, and provide further insight into, this phylogenetic view. Namely, a caudal shift of the forelimb-innervating MNs can be separated to two events: caudal shift of the boundary between the brachial and thoracic spinal cord, and acquisition of the apoptotic process in the cervical spinal cord for sculpting the MNs in the limb-free area. The requirement of the apoptotic process is probably due to some developmental constraints producing the forelimb-innervating MNs from the rostral-most level of the spinal cord. This could explain why the rostral and caudal borders of the brachial LMC are established by different mechanisms.

Development (2017) 144, 4645-4657 doi:10.1242/dev.158873

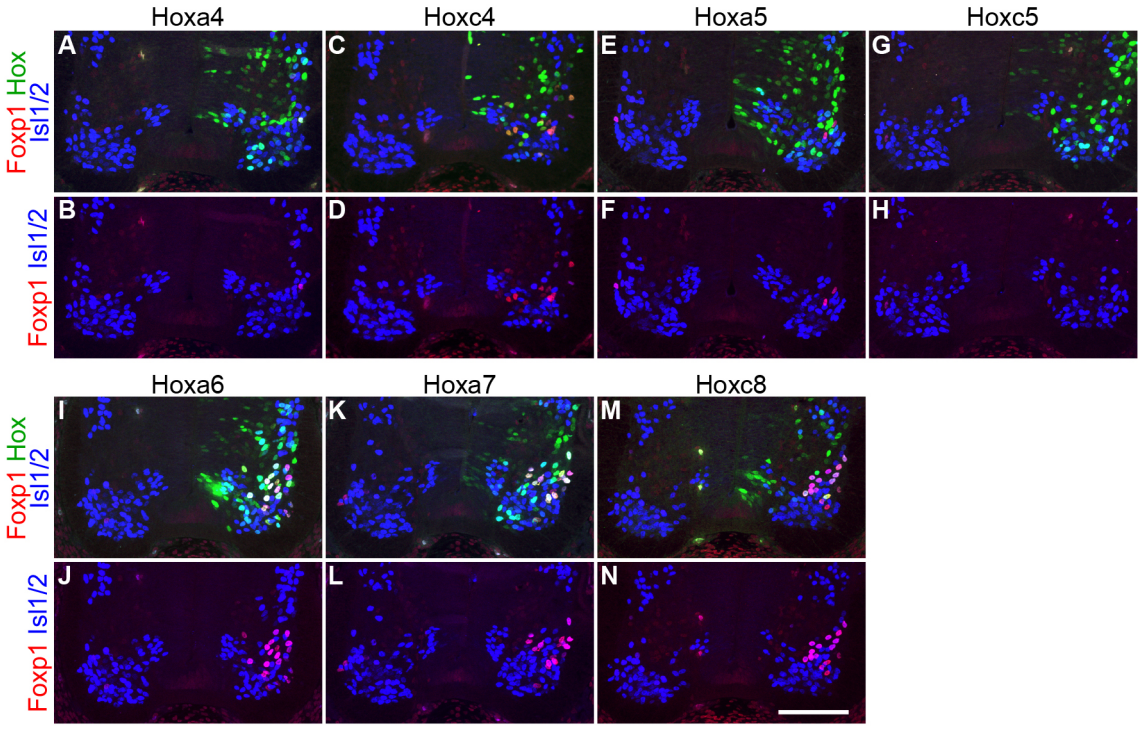

Fig. 7. Forced expression of Hox paralog group 6-8, but not 4-5, leads to the persistence of Foxp1$^+$ MNs in the cervical spinal cord. (A-N) V5- or Myc-tagged Hox genes were electroporated in the cervical region, and immunohistochemistry for V5, Foxp1, Isl1/2 (A,B,E-L) or Myc, Foxp1, Isl1/2 (C,D,M,N) was performed at HH27. Foxp1$^+$ MNs disappeared as in normal development after electroporation of *V5-Hoxa4* (A,B), *V5-Hoxa5* (E,F) and *V5-Hoxc5* (G,H). Only a few Foxp1$^+$ MNs were observed after electroporation of *Hoxc4-Myc* (C,D). The electroporation of *V5-Hoxa6* (I,J), *V5-Hoxa7* (K,L) and *Hoxc8-Myc* (M,N) resulted in the persistence of Foxp1$^+$ MNs. Scale bar: 100 µm (in N for A-N).

Mesodermal tissues as well as the MNs in the neck have unique properties

Limb muscles in amniotes as well as pectoral fin muscles in zebrafish are derived from migratory muscle precursors (MMPs), which de-epithelialize and actively migrate from ventrolateral lips of dermomyotome, and are marked by the expression of Lbx1 (Brohmann et al., 2000; Dietrich et al., 1998; Gross et al., 2000; Neyt et al., 2000). On the other hand, in the flank region, the intercostal muscles are generated by dermomyotome elongation; thus, Lbx1$^+$ MMPs are not formed. Notably, Lbx1 is also expressed in the dermomyotome of the cervical level, even though no limb or abaxial muscles are formed in this region (Dietrich et al., 1998). This rostrocaudal pattern of Lbx1 expression in the somitic mesoderm is analogous to that of Foxp1 expression in the spinal cord, and might be implicated in the caudal shift of the pectoral girdle in vertebrate evolution (Bothe et al., 2007).

When exogenous FGF is induced in the flank of chick embryo, an ectopic limb innervated by the spinal MNs of the flank level is generated, but this is not the case in the neck (Cohn et al., 1995; Lours and Dietrich, 2005; Turney et al., 2003). Thus, the neck is distinct from the flanks with respect to the competence to form a limb, though both the neck and flanks are limb-free areas. Lours and Dietrich suggested that a limb-incompetent state of lateral plate mesoderm and surface ectoderm in the neck is attributed to the interruption of the FGF signaling at distinct points (Lours and Dietrich, 2005). In addition to this, we propose that the non-limb-innervating state of MNs in the neck is attributable to apoptosis.

MATERIALS AND METHODS

Experimental animals

Fertilized chicken eggs were obtained from Takeuchi farm (Nara, Japan) and incubated at 38°C in a humidified incubator. Embryos were staged according to the Hamburger-Hamilton stage series (Hamburger and Hamilton, 1951). All animal experiments were performed in accordance with the Rules of Fukushima Medical University Animal Experiments, with approval of the Animal Experiments Committee of Fukushima Medical University.

Vector construction

The *Bcl-2* expression vector was constructed using a pMES vector, which contains chick β-actin promotor/CMV enhancer, an internal ribosome entry site, and *EGFP* sequences (Swartz et al., 2001). Custom oligonucleotides, including recognition sequences of *Cla*I, *Pac*I and *Mlu*I, were annealed and inserted into the *Eco*RI-*Sma*I site of the pMES vector. Custom oligonucleotides encoding a Myc epitope tag were inserted into the *Mlu*I-*Sma*I site of the pMES vector. Full-length *Bcl-2* was PCR-amplified from chick embryo cDNA, and was inserted into the *Eco*RI-*Mlu*I site of the pMES vector containing the *Myc* coding sequence. To construct shRNA expression vectors, custom oligonucleotides consisting of sense and antisense target sequences with an intervening loop sequence (Table S2) were annealed and inserted into pEGFPH1, which contains the human *H1* promoter for shRNA transcription and the CMV promoter for the expression of *EGFP* (Matsumoto et al., 2008). For *Foxp1* shRNA, five sequences of shRNA against chick *Foxp1* were designed (Table S3), and the knockdown efficiency of each shRNA-expression vector was evaluated by electroporation into the neural tube. One sequence that suppressed Foxp1 expression most effectively and did not cause any morphological damage to the spinal cord was selected as Foxp1-sh. Another sequence exhibiting neither knockdown effects nor morphological damage was selected as Cont-sh. For *Hoxc6* shRNA, the target sequence was based on the previous study, in which the effective target sequence of chick *Hoxc6* for RNAi has been reported (Dasen et al., 2005). For the construction of expression vector under the control of the *Hb9* regulatory element (pHb9), full-length chick *Foxp1* amplified by PCR and oligonucleotides encoding Myc epitope tag were inserted into an *Asc*I-linearized pHb9 vector using the In-Fusion HD Cloning Kit (Takara, Kyoto, Japan). Full-length *mCherry* was

Development (2017) 144, 4645-4657 doi:10.1242/dev.158873

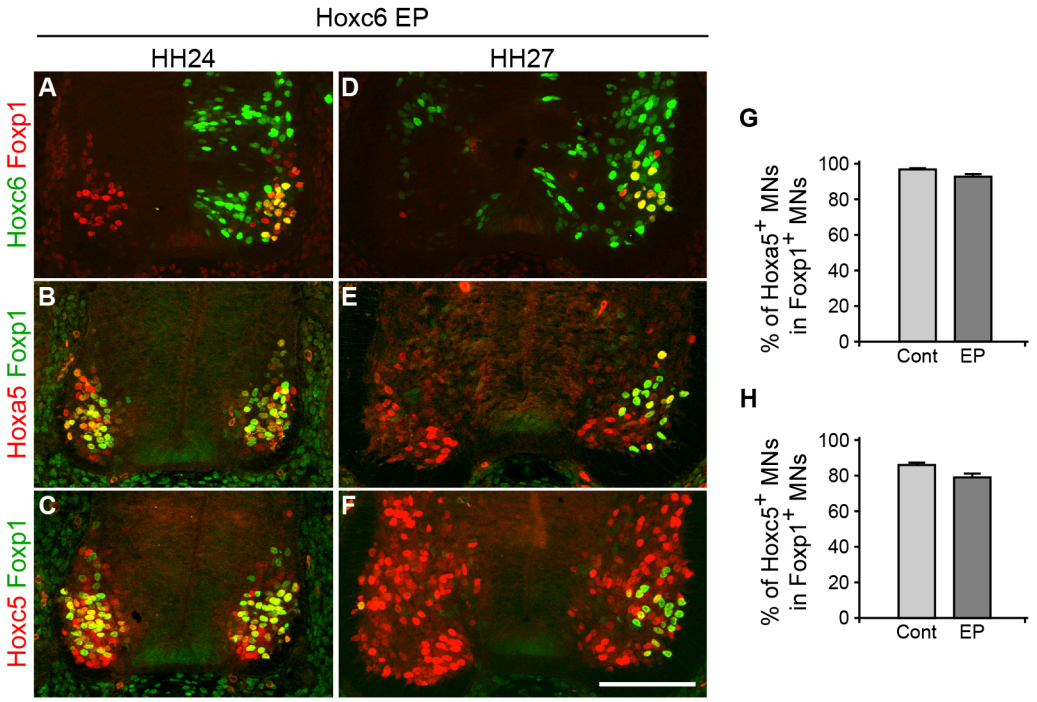

Fig. 8. Ectopic expression of Hoxc6 in the cervical spinal cord does not interfere with the expression of Hox paralog group 5 proteins. (A-F) *Hoxc6* was electroporated in the cervical region, and then immunohistochemistry for Hoxc6, Foxp1 (A,D), Hoxa5, Foxp1 (B,E), and Hoxc5, Foxp1 (C,F) was performed at HH24 or HH27. Hoxa5 and Hoxc5 were expressed in the majority of Foxp1$^+$ MNs both on the non-electroporated and *Hoxc6*-electroporated sides at HH24. Persistent Foxp1$^+$ MNs at HH27 after electroporation also expressed Hoxa5 and Hoxc5. (G,H) Quantification of Hoxa5$^+$ (G) or Hoxc5$^+$ (H) MNs at HH24 after *Hoxc6* electroporation. Percentages of Hoxa5$^+$ or Hoxc5$^+$ MNs in Foxp1$^+$ MNs on the non-electroporated (Cont) or electroporated (EP) side are shown. The percentages of Hoxa5$^+$ or Hoxc5$^+$ MNs were unaltered by Hoxc6 expression. *n*=10/3 (G), 10/4 (H). Values are mean±s.e.m. Two-tailed *t*-test. Scale bar: 100 µm (in F for A-F).

PCR-amplified from pmCherry-C1 (Takara), and inserted into the pHb9 vector as well. For pCAGGS-Foxp1-Myc, the *Foxp1-Myc* fragment was amplified from the pHb9-Foxp1-Myc vector and inserted into the *Eco*RI-linearized pCAGGS vector using the In-Fusion HD Cloning Kit (Takara). For construction of the Hoxc6 expression vector, full-length chick *Hoxc6* was PCR-amplified from chick embryo cDNA, and inserted into the *Cla*I-*Mlu*I site of the pMES vector. For construction of the expression vector for V5- or Myc-tagged Hox genes, full-length chick *Hoxa4*, *Hoxc4*, *Hoxa5*, *Hoxc5*, *Hoxa6*, *Hoxa7* and *Hoxc8* were PCR-amplified from chick embryo cDNA, and inserted into the pMES vector together with custom oligonucleotides encoding a V5 epitope tag, or into the pMES vector containing the *Myc* coding sequence, using the In-Fusion HD Cloning Kit (Takara). Construction of the Lhx3 expression vector is described in the supplementary Materials and Methods. The sequences of all primers used for PCR amplification are listed in Table S4.

In ovo electroporation

In ovo electroporation was performed as described previously (Sato et al., 2006), with slight modifications. Details are described in the supplementary Materials and Methods.

Retrograde tracing

Retrograde tracing was performed as described previously (Kobayashi et al., 2013).

Immunohistochemistry and TUNEL assay

Embryos were fixed in 0.1 M phosphate buffer/4% paraformaldehyde at 4°C overnight. Fixed embryos were cryoprotected in 20% sucrose at 4°C overnight, embedded in OCT compound, and cryosectioned. For immunohistochemistry, sections were boiled for 20 min in antigen retrieval solution (10 mM sodium citrate, 0.05% Tween 20, pH 6.0) and cooled down to room temperature. After washing with PBS/0.1% Triton X-100, the sections were incubated with primary antibodies at 4°C overnight, and with secondary antibodies for 1-2 h at room temperature. The antibodies are described in the supplementary Materials and Methods. For the TUNEL assay, sections were treated with 2 µg/ml proteinase K (Wako Pure Chemical Industries, Osaka, Japan) for 15 min, and the TUNEL reaction was performed as previously reported (Sato et al., 2002b). Alexa Fluor 488-, or 594-conjugated streptavidin (Thermo Fisher Scientific) was used for detection of incorporated biotin-16-dUTP. Whole-mount immunostaining was performed as described in the supplementary Materials and Methods. Images were captured using an Olympus BX51 fluorescence microscope equipped with an Olympus DP71 digital camera, or an Olympus FluoView FV1000 confocal microscope.

Cell culture and western blotting

pCAGGS-Foxp1-Myc and pEGFPH1 derivatives were co-transfected into human retinal pigment epithelial cell line ARPE-19 cells (kindly provided by T. Uemura, Fukushima Medical University, Japan) using FuGENE HD Transfection Reagent (Promega). After 24 h, the cells were collected, and the cell lysates were separated by SDS polyacrylamide gel electrophoresis and transferred to a PVDF membrane. Immunoblotting was performed with anti-Myc antibody (1:2000, sc-40, Santa Cruz Biotechnology) or anti-β-actin antibody (1:2000, A5441, Sigma-Aldrich).

Acknowledgements

We thank C. E. Krull, S. L. Pfaff, and C.-C. Hui for providing pMES, pHb9 and pEGFPH1 vectors, respectively; T. Uemura for providing ARPE-19 cells; M. Watanabe for technical guidance on antibody production; Y. Watanabe and M. Hashimoto for helpful comments and discussion. The monoclonal antibodies for Isl1/2, Lhx3, MNR2/Hb9 and Lhx1/5 developed by T. M. Jessell and S. Brenner-Morton, the monoclonal antibody for NF developed by T. M. Jessell, J. Dodd and S. Brenner-Morton, the monoclonal antibody for MyHC developed by D. A. Fischman, and the monoclonal antibody for Gag-Pro polyprotein developed by D. Boettiger were obtained from the Developmental Studies Hybridoma Bank, created by the NICHD of the NIH and maintained at The University of Iowa, Department of Biology, Iowa City, IA 52242, USA.

Competing interests
The authors declare no competing or financial interests.

Author contributions
Conceptualization: K.M., H.Y.; Methodology: K.M., N.S., H.Y.; Formal analysis: K.M., N.S., H.Y.; Investigation: K.M., C.S., T.O., N.S., H.Y.; Resources: T.O., T.S.; Writing - original draft: K.M.; Writing - review & editing: K.M., S.H., K.N., N.S., H.Y.; Funding acquisition: K.M., H.Y.

Funding
This work was supported by Japan Society for the Promotion of Science [JP25890016 to K.M., JP24500414, JP15K06741 to H.Y.].

Supplementary information
Supplementary information available online at
http://dev.biologists.org/lookup/doi/10.1242/dev.158873.supplemental

References

Agalliu, D., Takada, S., Agalliu, I., McMahon, A. P. and Jessell, T. M. (2009). Motor neurons with axial muscle projections specified by Wnt4/5 signaling. *Neuron* **61**, 708-720.
Arber, S., Han, B., Mendelsohn, M., Smith, M., Jessell, T. M. and Sockanathan, S. (1999). Requirement for the homeobox gene *Hb9* in the consolidation of motor neuron identity. *Neuron* **23**, 659-674.
Bel-Vialar, S., Itasaki, N. and Krumlauf, R. (2002). Initiating Hox gene expression: in the early chick neural tube differential sensitivity to FGF and RA signaling subdivides the *HoxB* genes in two distinct groups. *Development* **129**, 5103-5115.
Berggren, K., McCaffery, P., Dräger, U. and Forehand, C. J. (1999). Differential distribution of retinoic acid synthesis in the chicken embryo as determined by immunolocalization of the retinoic acid synthetic enzyme, RALDH-2. *Dev. Biol.* **210**, 288-304.
Bothe, I., Ahmed, M. U., Winterbottom, F. L., von Scheven, G. and Dietrich, S. (2007). Extrinsic versus intrinsic cues in avian paraxial mesoderm patterning and differentiation. *Dev. Dyn.* **236**, 2397-2409.
Brohmann, H., Jagla, K. and Birchmeier, C. (2000). The role of *Lbx1* in migration of muscle precursor cells. *Development* **127**, 437-445.
Burke, A. C., Nelson, C. E., Morgan, B. A. and Tabin, C. (1995). *Hox* genes and the evolution of vertebrate axial morphology. *Development* **121**, 333-346.
Cohn, M. J., Izpisúa-Belmonte, J. C., Abud, H., Heath, J. K. and Tickle, C. (1995). Fibroblast growth factors induce additional limb development from the flank of chick embryos. *Cell* **80**, 739-746.
Daeschler, E. B., Shubin, N. H. and Jenkins, F. A., Jr (2006). A Devonian tetrapod-like fish and the evolution of the tetrapod body plan. *Nature* **440**, 757-763.
Dasen, J. S. and Jessell, T. M. (2009). Hox networks and the origins of motor neuron diversity. *Curr. Top. Dev. Biol.* **88**, 169-200.
Dasen, J. S., Liu, J.-P. and Jessell, T. M. (2003). Motor neuron columnar fate imposed by sequential phases of Hox-c activity. *Nature* **425**, 926-933.
Dasen, J. S., Tice, B. C., Brenner-Morton, S. and Jessell, T. M. (2005). A Hox regulatory network establishes motor neuron pool identity and target-muscle connectivity. *Cell* **123**, 477-491.
Dasen, J. S., De Camilli, A., Wang, B., Tucker, P. W. and Jessell, T. M. (2008). Hox repertoires for motor neuron diversity and connectivity gated by a single accessory factor, FoxP1. *Cell* **134**, 304-316.
Dietrich, S., Schubert, F. R., Healy, C., Sharpe, P. T. and Lumsden, A. (1998). Specification of the hypaxial musculature. *Development* **125**, 2235-2249.
Ensini, M., Tsuchida, T. N., Belting, H. G. and Jessell, T. M. (1998). The control of rostrocaudal pattern in the developing spinal cord: specification of motor neuron subtype identity is initiated by signals from paraxial mesoderm. *Development* **125**, 969-982.
Ericsson, R., Knight, R. and Johanson, Z. (2013). Evolution and development of the vertebrate neck. *J. Anat.* **222**, 67-78.
Francius, C. and Clotman, F. (2014). Generating spinal motor neuron diversity: a long quest for neuronal identity. *Cell. Mol. Life Sci.* **71**, 813-829.
Gross, M. K., Moran-Rivard, L., Velasquez, T., Nakatsu, M. N., Jagla, K. and Goulding, M. (2000). *Lbx1* is required for muscle precursor migration along a lateral pathway into the limb. *Development* **127**, 413-424.
Hamburger, V. and Hamilton, H. L. (1951). A series of normal stages in the development of the chick embryo. *J. Morphol.* **88**, 49-92.
Janvier, P. (1996). *Early Vertebrates*. Oxford, UK: Clarendon Press.
Jarrar, W., Dias, J. M., Ericson, J., Arnold, H.-H. and Holz, A. (2015). Nkx2.2 and Nkx2.9 are the key regulators to determine cell fate of branchial and visceral motor neurons in caudal hindbrain. *PLoS ONE* **10**, e0124408.
Jessell, T. M. (2000). Neuronal specification in the spinal cord: inductive signals and transcriptional codes. *Nat. Rev. Genet.* **1**, 20-29.
Jung, H., Lacombe, J., Mazzoni, E. O., Liem, K. F., Jr, Grinstein, J., Mahony, S., Mukhopadhyay, D., Gifford, D. K., Young, R. A., Anderson, K. V. et al. (2010). Global control of motor neuron topography mediated by the repressive actions of a single *Hox* gene. *Neuron* **67**, 781-796.
Jung, H., Mazzoni, E. O., Soshnikova, N., Hanley, O., Venkatesh, B., Duboule, D. and Dasen, J. S. (2014). Evolving *Hox* activity profiles govern diversity in locomotor systems. *Dev. Cell* **29**, 171-187.
Kobayashi, N., Homma, S., Okada, T., Masuda, T., Sato, N., Nishiyama, K., Sakuma, C., Shimada, T. and Yaginuma, H. (2013). Elucidation of target muscle and detailed development of dorsal motor neurons in chick embryo spinal cord. *J. Comp. Neurol.* **521**, 2987-3002.
Lance-Jones, C., Omelchenko, N., Bailis, A., Lynch, S. and Sharma, K. (2001). *Hoxd10* induction and regionalization in the developing lumbosacral spinal cord. *Development* **128**, 2255-2268.
Levi-Montalcini, R. (1950). The origin and development of the visceral in the spinal cord of the chick embryo. *J. Morphol.* **86**, 253-283.
Liu, J.-P., Laufer, E. and Jessell, T. M. (2001). Assigning the positional identity of spinal motor neurons: rostrocaudal patterning of Hox-c expression by FGFs, Gdf11, and retinoids. *Neuron* **32**, 997-1012.
Lours, C. and Dietrich, S. (2005). The dissociation of the Fgf-feedback loop controls the limbless state of the neck. *Development* **132**, 5553-5564.
Lumsden, A. (1995). Neural development. A 'LIM code' for motor neurons? *Curr. Biol.* **5**, 491-495.
Luxenhofer, G., Helmbrecht, M. S., Langhoff, J., Giusti, S. A., Refojo, D. and Huber, A. B. (2014). MicroRNA-9 promotes the switch from early-born to late-born motor neuron populations by regulating Onecut transcription factor expression. *Dev. Biol.* **386**, 358-370.
Ma, L.-H., Gilland, E., Bass, A. H. and Baker, R. (2010). Ancestry of motor innervation to pectoral fin and forelimb. *Nat. Commun.* **1**, 49.
Matsumoto, K., Miki, R., Nakayama, M., Tatsumi, N. and Yokouchi, Y. (2008). Wnt9a secreted from the walls of hepatic sinusoids is essential for morphogenesis, proliferation, and glycogen accumulation of chick hepatic epithelium. *Dev. Biol.* **319**, 234-247.
Misra, M., Shah, V., Carpenter, E., McCaffery, P. and Lance-Jones, C. (2009). Restricted patterns of Hoxd10 and Hoxd11 set segmental differences in motoneuron subtype complement in the lumbosacral spinal cord. *Dev. Biol.* **330**, 54-72.
Mizuguchi, R., Sugimori, M., Takebayashi, H., Kosako, H., Nagao, M., Yoshida, S., Nabeshima, Y., Shimamura, K. and Nakafuku, M. (2001). Combinatorial roles of olig2 and neurogenin2 in the coordinated induction of pan-neuronal and subtype-specific properties of motoneurons. *Neuron* **31**, 757-771.
Morikawa, Y., Komori, T., Hisaoka, T. and Senba, E. (2009). Detailed expression pattern of Foxp1 and its possible roles in neurons of the spinal cord during embryogenesis. *Dev. Neurosci.* **31**, 511-522.
Nagashima, H., Sugahara, F., Watanabe, K., Shibata, M., Chiba, A. and Sato, N. (2016). Developmental origin of the clavicle, and its implications for the evolution of the neck and the paired appendages in vertebrates. *J. Anat.* **229**, 536-548.
Neyt, C., Jagla, K., Thisse, C., Thisse, B., Haines, L. and Currie, P. D. (2000). Evolutionary origins of vertebrate appendicular muscle. *Nature* **408**, 82-86.
Novitch, B. G., Chen, A. I. and Jessell, T. M. (2001). Coordinate regulation of motor neuron subtype identity and pan-neuronal properties by the bHLH repressor Olig2. *Neuron* **31**, 773-789.
O'Connor, T. M. and Wyttenbach, C. R. (1974). Cell death in the embryonic chick spinal cord. *J. Cell Biol.* **60**, 448-459.
Omelchenko, N. and Lance-Jones, C. (2003). Programming neural *Hoxd10*: in vivo evidence that early node-associated signals predominate over paraxial mesoderm signals at posterior spinal levels. *Dev. Biol.* **261**, 99-115.
Philippidou, P. and Dasen, J. S. (2013). Hox genes: choreographers in neural development, architects of circuit organization. *Neuron* **80**, 12-34.
Philippidou, P., Walsh, C. M., Aubin, J., Jeannotte, L. and Dasen, J. S. (2012). Sustained *Hox5* gene activity is required for respiratory motor neuron development. *Nat. Neurosci.* **15**, 1636-1644.
Roncali, L. (1970). The brachial plexus and the wing nerve pattern during early developmental phases in chicken embryos. *Monit. Zool. Ital.* **4**, 81-98.
Rousso, D. L., Gaber, Z. B., Wellik, D., Morrisey, E. E. and Novitch, B. G. (2008). Coordinated actions of the forkhead protein Foxp1 and Hox proteins in the columnar organization of spinal motor neurons. *Neuron* **59**, 226-240.
Sato, N., Matsuda, K., Sakuma, C., Foster, D. N., Oppenheim, R. W. and Yaginuma, H. (2002a). Regulated gene expression in the chicken embryo by using replication-competent retroviral vectors. *J. Virol.* **76**, 1980-1985.
Sato, N., Sakuma, C., Kato, H., Milligan, C. E., Oppenheim, R. W. and Yaginuma, H. (2002b). Bcl-2 rescues motoneurons from early cell death in the cervical spinal cord of the chicken embryo. *J. Neurobiol.* **53**, 381-390.
Sato, N., Sakuma, C., Sato, Y., Gould, T. W., Oppenheim, R. W. and Yaginuma, H. (2006). Distinct susceptibility of developing neurons to death following Bax overexpression in the chicken embryo. *Cell Death Differ.* **13**, 435-445.
Shah, V., Drill, E. and Lance-Jones, C. (2004). Ectopic expression of Hoxd10 in thoracic spinal segments induces motoneurons with a lumbosacral molecular profile and axon projections to the limb. *Dev. Dyn.* **231**, 43-56.
Shieh, P. (1951). The neoformation of cells of preganglionic type in the cervical spinal cord of the chick embryo following its transplantation to the thoracic level. *J. Exp. Zool.* **117**, 359-395.

Development (2017) 144, 4645-4657 doi:10.1242/dev.158873

Shubin, N. H., Daeschler, E. B. and Jenkins, F. A., Jr (2006). The pectoral fin of *Tiktaalik roseae* and the origin of the tetrapod limb. *Nature* **440**, 764-771.

Stifani, N. (2014). Motor neurons and the generation of spinal motor neuron diversity. *Front. Cell. Neurosci.* **8**, 293.

Swartz, M. E., Eberhart, J., Pasquale, E. B. and Krull, C. E. (2001). EphA4/ephrin-A5 interactions in muscle precursor cell migration in the avian forelimb. *Development* **128**, 4669-4680.

Thaler, J., Harrison, K., Sharma, K., Lettieri, K., Kehrl, J. and Pfaff, S. L. (1999). Active suppression of interneuron programs within developing motor neurons revealed by analysis of homeodomain factor HB9. *Neuron* **23**, 675-687.

Tsuchida, T., Ensini, M., Morton, S. B., Baldassare, M., Edlund, T., Jessell, T. M. and Pfaff, S. L. (1994). Topographic organization of embryonic motor neurons defined by expression of LIM homeobox genes. *Cell* **79**, 957-970.

Turney, B. W., Rowan-Hull, A. M. and Brown, J. M. (2003). The innervation of FGF-induced additional limbs in the chick embryo. *J. Anat.* **202**, 83-92.

Watanabe, M., Fukaya, M., Sakimura, K., Manabe, T., Mishina, M. and Inoue, Y. (1998). Selective scarcity of NMDA receptor channel subunits in the stratum lucidum (mossy fibre-recipient layer) of the mouse hippocampal CA3 subfield. *Eur. J. Neurosci.* **10**, 478-487.

Wellik, D. M. (2007). Hox patterning of the vertebrate axial skeleton. *Dev. Dyn.* **236**, 2454-2463.

Wu, Y., Wang, G., Scott, S. A. and Capecchi, M. R. (2008). Hoxc10 and Hoxd10 regulate mouse columnar, divisional and motor pool identity of lumbar motoneurons. *Development* **135**, 171-182.

Yaginuma, H., Tomita, M., Takashita, N., McKay, S. E., Cardwell, C., Yin, Q.-W. and Oppenheim, R. W. (1996). A novel type of programmed neuronal death in the cervical spinal cord of the chick embryo. *J. Neurosci.* **16**, 3685-3703.

Yaginuma, H., Shiraiwa, N., Shimada, T., Nishiyama, K., Hong, J., Wang, S., Momoi, T., Uchiyama, Y. and Oppenheim, R. W. (2001). Caspase activity is involved in, but is dispensable for, early motoneuron death in the chick embryo cervical spinal cord. *Mol. Cell. Neurosci.* **18**, 168-182.